Populations of $n = 2$ states of atomic hydrogen in low-density hydrogen plasma: temperature and metastability of $2s^2S_{1/2}$

Shusuke Nishiyama[1] **and Koichi Sasaki**[2]‡

[1]Faculty of Health Science, Japan Healthcare University, 1-50, 11-choume, Tsukisamu-Higashi 3-jo, Toyohira-ku, Sapporo, 062-0053, Japan

[2]Division of Applied Quantum Science and Engineering, Hokkaido University, Sapporo 060-8628, Japan

E-mail: sasaki@qe.eng.hokudai.ac.jp

Abstract. The populations of the $2s^2S_{1/2}$, $2p^2P_{1/2}$, and $2p^2P_{3/2}$ states of atomic hydrogen were examined in a low-density inductively coupled hydrogen plasma using diode laser absorption spectroscopy at the Balmer-α line. The Doppler broadened absorption spectra were not fitted with the theoretical spectra under the assumption that the population distribution of the three states followed the statistical weights. The fitting accuracy improved when the population ratio was allowed to deviate from the statistical weights; however, the improvement remained insufficient, especially for spectra observed at low electron densities and low hydrogen pressures. A reasonable fit was achieved only when a high-temperature component was introduced into the velocity distribution function of the $2s^2S_{1/2}$ state. It was considered that the high-temperature component was produced via the electron-impact dissociative excitation of molecular hydrogen, because the population of the high-temperature component was proportional to the electron density. The experimental results clearly indicated a decrease in the population of high-temperature $2s^2S_{1/2}$ with increasing electron density and hydrogen pressure. This trend is qualitatively reasonable considering the collisional transfer from the $2s^2S_{1/2}$ to the $2p^2P_{1/2}$ and $2p^2P_{3/2}$ states. However, the cross-sections of the collisional transfer were insufficiently small to explain the experimental observations quantitatively. In addition, the experimental results suggest lower metastability of low-temperature $2s^2S_{1/2}$ than that of the high-temperature component, which cannot be explained by collision cross-sections. Thus, a more sophisticated model should be investigated in future studies to obtain a deeper understanding of the kinetics governing the $2s^2S_{1/2}$, $2p^2P_{1/2}$, and $2p^2P_{3/2}$ states.

Submitted to: *Plasma Sources Sci. Technol.*

1. Introduction

The first excited state of atomic hydrogen with $n = 2$, where n is the principal quantum number, is composed of three sub-levels: $2s^2S_{1/2}$, $2p^2P_{1/2}$, and $2p^2P_{3/2}$. The $2p^2P_{1/2}$ and

‡ Author to whom any correspondence should be addressed.

$2p^2P_{3/2}$ states are connected to the ground state ($1s^2S_{1/2}$) optically by the Lyman-α transition with a high transitions probability of 6.3×10^8 s^{-1} [1], whereas the $2s^2S_{1/2}$ state is a metastable state. Since transition probabilities of the single- and two-photon emissions between $1s^2S_{1/2}$ and $2s^2S_{1/2}$ is 2.5×10^{-6} s^{-1} [1] and 8.2 s^{-1} [2], respectively, the lifetime of the $2s^2S_{1/2}$ state is longer than 0.1 s in the collisionless condition. However, if the $2s^2S_{1/2}$ state is produced in a plasma, it is transferred to the $2p^2P_{1/2}$ and $2p^2P_{3/2}$ states by collisions, followed by the Lyman-α transition to the ground state. Thus, "the metastability" of the $2s^2S_{1/2}$ state in plasma is determined by collisions. Since the energy difference between the $2s^2S_{1/2}$ and $2p^2P_{3/2}$ states is less than 0.4 cm^{-1} [1], collisions with electron as well as neutral species can contribute to the collisional transition.

As described above, the population distribution among the $2s^2S_{1/2}$, $2p^2P_{1/2}$, and $2p^2P_{3/2}$ states of atomic hydrogen in plasma is an interesting issue from the fundamental perspective. A convenient method for investigating the populations of the $2s^2S_{1/2}$, $2p^2P_{1/2}$, and $2p^2P_{3/2}$ states experimentally is to measure the absorption spectrum of the Balmer-α line by single-mode laser absorption spectroscopy. A partial energy-level diagram of atomic hydrogen is shown in Fig. 1. As the $n = 3$ state of atomic hydrogen is composed of five sub-levels ($3s^2S_{1/2}$, $3p^2P^o_{1/2}$, $3p^2P^o_{3/2}$, $3d^2D_{3/2}$, and $3d^2D_{5/2}$), the Balmer-α line is composed of seven fine-structure components according to the selection rule. In the following sections, we have specified the seven transitions using labels A-G, as shown in Fig. 1. Table 1 summarizes the wavelengths and the transition probabilities of the fine-structure components together with the energy states. Because the wavelength differences between the transition lines are smaller than the Doppler width when the temperature of atomic hydrogen is higher than room temperature, the seven lines with Doppler broadening overlap. However, it is possible to evaluate the populations of the $2s^2S_{1/2}$, $2p^2P_{1/2}$, and $2p^2P_{3/2}$ states by the spectral fitting based on the superposition of the Doppler-broadened seven transition lines.

The laser absorption spectra of the Balmer-α line of atomic hydrogen have been reported by several authors [3–10]. Most authors reported that their absorption spectra agreed well with the theoretical spectra under the assumption that $2s^2S_{1/2}$, $2p^2P_{1/2}$, and $2p^2P_{3/2}$ had the same Doppler width, and that the population distribution among the three states was equal to the statistical weights [4, 6–10]. This implies that the metastability of the $2s^2S_{1/2}$ state was negligible. However, Biraben *et al.* [3] and Lipp and O'Brien [5] reported the absorption spectra that were not fitted by the population distribution according to the statistical weights. In particular, Lipp and O'Brien reported that the spectra they observed in a capacitively coupled radio frequency (RF) plasma could be fitted with theoretical spectra when they assumed two temperatures in the velocity distribution functions of the three states [5]. In addition, they assumed a population distribution based on the statistical weights for the low-temperature component, whereas they required a population distribution that deviated from the statistical weights for the high-temperature component.

Optical emission spectra with "super-hot" hydrogen atoms have been observed in various plasmas at Balmer lines by many researchers [11–18]. The mechanism of super-hot hydrogen atoms is the back-scattering of hydrogen ions on the cathode surface followed by dissociation or charge exchange collision. Another type of fast hydrogen atoms, which are hotter than

thermal hydrogen atoms but much colder than the super-hot hydrogen atoms mentioned above, are produced via the dissociative excitation of molecular hydrogen. Leventhal *et al.* [19], Misakian and Zorn [20], and Ryan *et al.* [21] detected fast $2s^2S_{1/2}$ produced by dissociative excitation using time-of-flight techniques. The high-temperature components originated from dissociative excitation were also observed in the optical emission spectra of the Lyman-α line [22], the Lyman-β line [23], and the Balmer lines [24,25]. However, the results in [19–25] were obtained through collision experiments using electron beams and were not obtained in plasmas.

In the present work, we examined the Doppler-broadened laser absorption spectrum at the Balmer-α line of atomic hydrogen in a low-density inductively coupled plasma source. In addition, saturated absorption spectroscopy was used to obtain the Doppler-free spectrum. The Doppler-broadened absorption spectra were not able to be fitted with the theoretical spectra under the assumption that the population distribution among the $2s^2S_{1/2}$, $2p^2P_{1/2}$, and $2p^2P_{3/2}$ states was equal to the statistical weights. In addition, the experimental absorption spectra were not fitted by the single Doppler width for the seven transition lines, even though we assumed the population distribution deviated from the statistical weights. The reasonable fitting was obtained only when we assumed the population densities deviated from the statistical weights and a high-temperature component for the velocity distribution function of the $2s^2S_{1/2}$ state. We discuss the metastability of the $2s^2S_{1/2}$ state and the contribution of dissociative excitation to the absorption spectra based on experimental observations.

The remainder of this paper is organized as follows. In Section 2, details of the experimental apparatus and methods are described. Section 3 presents the experimental results on the spectral fitting and the populations of the $2s^2S_{1/2}$, $2p^2P_{1/2}$, and $2p^2P_{3/2}$ states. In Section 4, we compare the experimental results with the available collision cross sections. Finally, the present work is summarized in Section 5.

2. Experiment

The experimental apparatus is schematically shown in Fig. 2. Inductively coupled plasmas (ICP) were produced in a cylindrical vacuum chamber with a diameter and height of 26 cm. Pure hydrogen was introduced into the vacuum chamber after evacuating it below 4×10^{-6} Torr using a turbomolecular pump. The hydrogen pressure was varied between 10 and 80 mTorr as measured using a capacitance manometer. A one-turn RF antenna was inserted into the vacuum chamber and connected to an RF power supply at 13.56 MHz via a matching circuit. The RF antenna was electrically insulated from the plasma by covering its surface with glass fibers. The RF power was modulated on and off at a frequency of 5 kHz. The instantaneous power was varied between 0.2 and 1 kW with a duty factor of 50%.

A linearly-polarized, single-mode, tunable diode laser was used for measuring the absorption spectrum of the Balmer-α line of atomic hydrogen. The output power of the diode laser was approximately 13.4 mW. A Fabry-Perot spectrum analyzer with a free spectral range of 1 GHz was used to monitor the wavelength of the scanning laser. A mode hop-free tuning range of approximately 40 GHz was possible around the Balmer-α line of atomic

hydrogen (656.3 nm). The laser linewidth was estimated to be 1 MHz, which was narrower than the natural and Doppler widths of the transitions. The output from the diode laser was divided into two beams after passing through an optical isolator, and both the laser beams were injected into optical fibers. The diode laser beams exiting the optical fibers were collimated and injected into the plasma on the same optical axis from counter directions. In saturated absorption spectroscopy, a weaker laser beam (approximately 0.41 mW), which was picked up using a glass plate, was used as the probe beam, while an intense laser beam (approximately 5.3 mW) was used as the pump beam. We carefully verified that the probe and pump beams perfectly overlapped at the optical windows on both sides of the vacuum chamber. The probe beam transmitted through the plasma was detected using a photodiode and the electrical signal from the photodiode was connected to a lock-in amplifier. An interference filter was placed in front of the photodiode to eliminate the optical emissions from the plasma at wavelengths other than the Balmer-α line. The optical emission from the plasma at the Balmer-α line was also detected by the photodiode, but it did not affect the absorption spectrum because of the negligible intensity. The two irises with diameters of 1.5 mm were effective in reducing the optical emission intensity arriving at the photodiode. When the Doppler-broadened absorption spectrum was measured, the pump beam was blocked, and the intensity of the transmitted probe beam was recorded as a function of the scanning laser wavelength. The lock-in amplifier with the reference frequency equal to the modulation frequency of the RF power (5 kHz) was utilized to amplify the difference between the transmitted laser intensities with and without the plasma, and as a result, we succeeded in recording the weak absorption spectrum. In saturated absorption spectroscopy, both the probe and pump beams were injected into the plasma. In this case, the Lamb dips with a Doppler-free spectral resolution, which indicated the locations of the centers of the transition lines, were superposed on the Doppler-broadened absorption spectrum of the probe beam. The Lamb-dip spectrum was obtained from the difference between the absorption spectra with and without the pump beam.

3. Results

3.1. Plasma parameters

The electron density and electron temperature, which were measured at the center of the plasma region using a Langmuir probe, are shown in Fig. 3 as functions of the RF power. The measurements were repeated at hydrogen pressures of 10, 20, and 40 mTorr. The error bars show the uncertainty in deducing the electron temperature and electron density from the relationship between the potential and current of the Langmuir probe. The electron density ranged between 10^{14} and 10^{16} m^{-3}, as shown in Fig. 3(a). A density jump from the capacitively coupled plasma (CCP) to the ICP modes was observed at an RF power between 300 and 400 W when the hydrogen pressure was 10 mTorr, whereas ICP mode discharges were obtained at 300 W when the hydrogen pressures were 20 and 40 mTorr. The discharges at 200 W were excluded from the experimental conditions when the hydrogen pressures were 20 and 40 mTorr because it was difficult to realize reproducible discharges. The electron

density after the density jump was still on the order of 10^{15} m^{-3}. This electron density is lower than that of argon ICP discharges, but the lower density may be due to the fact that the plasma was produced using pure hydrogen. The electron temperature ranged between 1 and 3 eV, as shown in Fig. 3(b).

3.2. Absorption spectrum and its fitting

Figure 4(a) shows the Doppler-broadened absorption spectrum observed at an RF power of 700 W and a hydrogen pressure of 40 mTorr. The origin of the horizontal axis in Fig. 4 is chosen at the line center frequency of transition C ($2p^2P_{3/2}$-$3d^2D_{5/2}$). The vertical axis is the absorption A given by $A = 1 - I_t/I_0$ with I_0 and I_t being the incident and transmitted laser intensities, respectively. The weak absorption on the order of $10^{-5} - 10^{-4}$ was clearly observed with the help of the lock-in amplifier. According to the Lambert-Beer law, absorption is given by

$$A(\nu) = 1 - \frac{I_t(\nu)}{I_0(\nu)} = 1 - \exp\left\{-\sum_i \sigma_i(\nu) n_i l\right\} \simeq \sum_i \sigma_i(\nu) n_i l, \tag{1}$$

where $\sigma_i(\nu)$ and n_i are the absorption cross section and the population of the lower energy state of the ith transition, respectively, and l is the absorption length. The amplitude of $\sigma_i(\nu)$ was obtained from the transition probability and the statistical weights [26], and we assumed a Gaussian (or Doppler) distribution for the lineshape of $\sigma_i(\nu)$. The laser linewidth was much narrower than the Doppler width. Figure 4(c) shows the Lamb dip spectrum obtained from the difference between the spectrum shown in Fig. 4(a) and that of saturated absorption spectroscopy. Although the Balmer-α line is composed of seven transitions, only four peaks (C, D, F, and G) were clearly visible in the Lamb dip spectrum. The main reason for the other peaks (A, B, and E) having amplitudes below the detection limit is the small transition probabilities. Peak X represents the cross-over between peaks D and F, which is an unavoidable parasitic peak in saturated absorption spectroscopy [27].

The theoretical spectra obtained under the following assumptions are shown in Fig. 4(a). In fitting model (i), we assumed a single Doppler width for the seven transitions and the population distribution according to the statistical weights for the $2s^2S_{1/2}$, $2p^2P_{1/2}$, and $2p^2P_{3/2}$ states. As shown in the residue spectrum (Fig. 4(b)), the fitting result of model (i) is insufficient, and a substantial residue is observed between the experimental and theoretical absorption spectra. In fitting model (ii), we assumed a single Doppler width for the seven transitions, but we relaxed the limitation in the population distribution. The fitting was improved by treating the population distribution as an additional fitting parameter but it was still insufficient, as shown in Fig. 4(b). The negative residue in the positive-frequency wing (13-23 GHz) suggests the existence of a high-temperature component. In fitting model (iii), we assumed two Doppler widths for transitions D and F with keeping the population distribution deviated from the statistical weights. Specifically, the high- and low-temperature components were assumed in the velocity distribution function of the $2s^2S_{1/2}$ state and a single temperature equal to the low-temperature component of $2s^2S_{1/2}$ was assumed in the velocity distribution functions of the $2p^2P_{1/2}$ and $2p^2P_{3/2}$ states. The experimental absorption

spectrum was reproduced well by fitting model (iii). The difference in the fitting results is seen in the example shown in Fig. 5, which was observed at an RF power of 700 W and a hydrogen pressure of 10 mTorr, more clearly. The absorption spectrum in Fig. 5(a) is considerably different from that in Fig. 4(a). The Lamb-dip spectrum shown in Fig. 5(c) indicates that transition C was weaker and transitions D and F were more intense than the Lamb-dip spectrum shown in Fig. 4(c). In this case, fitting model (i) resulted in a significant residue, as shown in Fig. 5(b). This is because model (i) assumes the highest population for $2p^2P_{3/2}$ because it has the largest statistical weight. In addition, the fitting result obtained by model (ii) was also insufficient significantly, as shown in Fig. 5(b). Model (iii) provides a reasonable fit to the experimental absorption spectrum.

3.3. Temperatures

As shown in Figs. 4 and 5, the experimental absorption spectra were fitted reasonably by fitting model (iii), which assumed population distribution deviated from the statistical weights and a high-temperature component in the velocity distribution function of the $2s^2S_{1/2}$ state. Figure 6 summarizes the temperatures evaluated by spectral fitting using model (iii). The error bars indicate the uncertainty of the spectral fitting. Error bars are smaller than the plot symbols if they are not shown in the figure. The high-temperature component of the velocity distribution function of the $2s^2S_{1/2}$ state ranged from 2000 K to 3000 K, whereas the low-temperature component was approximately 400 K.

3.4. Population distribution

The populations of the high-temperature component of the $2s^2S_{1/2}$ state and the low-temperature components of the $2s^2S_{1/2}$, $2p^2P_{1/2}$, and $2p^2P_{3/2}$ states are plotted in Fig. 7 as functions of the electron density. Figure 8 shows their fractional abundances or ratios in the total population of the $n = 2$ state. As shown in Figs. 7 and 8, the $2s^2S_{1/2}$ state with the high temperature was dominant at low hydrogen pressures and low electron densities. The fractional abundance of high-temperature $2s^2S_{1/2}$ decreased steeply with hydrogen pressure and electron density, as shown in Figs. 8(a)-8(c), and the population of the high-temperature $2s^2S_{1/2}$ state was negligible at a hydrogen pressure of 80 mTorr (hence, it is not plotted in Figs. 7(d) and 8(d)). The fractional abundances of the $2s^2S_{1/2}$, $2p^2P_{1/2}$, and $2p^2P_{3/2}$ states were independent of the electron density at 80 mTorr, as shown in Fig. 8(d), and were close to the statistical weights (0.5 of $2p^2P_{3/2}$ and 0.25 of $2s^2S_{1/2}$ and $2p^2P_{1/2}$). This means that the absorption spectra observed at 80 mTorr were roughly approximated by fitting model (i), which is a similar result to the majority of papers to date [4, 6–10]. Another important point that should be noted is the dotted curves in Fig. 7. As shown in Fig. 7, the population of high-temperature $2s^2S_{1/2}$ was proportional to electron density, whereas the populations of $2p^2P_{1/2}$, $2p^2P_{3/2}$, and low-temperature $2s^2S_{1/2}$ were proportional to the square of the electron density.

4. Discussion

4.1. Metastability of $2s^2S_{1/2}$

Although most studies available to date have reported negligible metastability of $2s^2S_{1/2}$ in plasmas [4, 6–10], we observed that the population of high-temperature $2s^2S_{1/2}$ was higher than the statistical weight, as shown in Fig. 8, at a low electron density ($n_e \leq 1 \times 10^{16}$ m^{-3}) and a low hydrogen pressure ($P \leq 20$ mTorr). The metastability of the $2s^2S_{1/2}$ state is disturbed by collisions, and electrons and molecular hydrogen can contribute to the collisional loss of $2s^2S_{1/2}$. According to Janev *et al.* [28], the rate coefficient for $H(2s)+e \rightarrow H(2p)+e$ is $(4-8) \times 10^{-12}$ m^3/s at an electron temperature of 1-2 eV. Hence, the frequency of collisional transfer from $2s^2S_{1/2}$ to $2p^2P_{1/2}$ and $2p^2P_{3/2}$ is estimated to be less than 2×10^5 s^{-1} at an electron density of $n_e = 2 \times 10^{16}$ m^{-3}. Since this frequency is significantly lower than the decay frequencies of $2p^2P_{1/2}$ and $2p^2P_{3/2}$ (that is, the transition probability of the Lyman-α line), it is expected that the collision with electron does not disturb the metastability of $2s^2S_{1/2}$, and a higher population of $2s^2S_{1/2}$ than the statistical weight is observed even at an electron density higher than 10^{16} m^{-3}. However, according to the experimental result shown in Fig. 8, the metastability of $2s^2S_{1/2}$ is disturbed at $n_e \geq 2 \times 10^{16}$ m^{-3}, which cannot be explained by collision with electrons.

The cross-section of collisional quenching of $2s^2S_{1/2}$ by molecular hydrogen has been reported in several papers [29–32], and it ranges between 1×10^{-18} and 1.5×10^{-18} m^2 at a mean thermal velocity of 7×10^3 m/s corresponding 2500 K. The cross-section corresponds to a collision frequency of 2×10^7 s^{-1} at a hydrogen pressure of 80 mTorr. To estimate the density of molecular hydrogen, which was necessary for estimating the collision frequency, we assumed a temperature equal to that of the low-temperature components of $2s^2S_{1/2}$, $2p^2P_{1/2}$, and $2p^2P_{3/2}$ (400 K). Since the quenching frequency is more than one order of magnitude lower than the transition probability of the Lyman-α line, it is considered that the $2s^2S_{1/2}$ state can keep its metastability even at 80 mTorr, whereas the experimental result shown in Fig. 8(d) shows the negligible metastability.

Another point that remains difficult to explain is the difference between the metastabilities of the high- and low-temperature $2s^2S_{1/2}$, as shown in Figs. 8(b) and 8(c) (20 and 40 mTorr). The population of low-temperature $2s^2S_{1/2}$ is close to the population of $2p^2P_{1/2}$ and is roughly half of the population of $2p^2P_{3/2}$ even at electron densities less than 1×10^{16} m^{-3}. The population distribution was close to the statistical weights, indicating that the metastability of low-temperature $2s^2S_{1/2}$ was disturbed even at a low electron density and low hydrogen pressure, whereas high-temperature $2s^2S_{1/2}$ can maintain its metastability. Note that a similar collision frequency is expected for the quenching of low-temperature $2s^2S_{1/2}$ by molecular hydrogen, considering the differences in the cross-section and mean thermal velocity. In addition, considering the van der Waals radius of atomic hydrogen [33], the energy relaxation of high-temperature $2s^2S_{1/2}$ by elastic collision with molecular hydrogen may have a frequency close to 10^7 s^{-1}; however, we did not observe low-temperature $2s^2S_{1/2}$ with the metastability transferred from high-temperature $2s^2S_{1/2}$. This trend also suggests a

more significant disturbance of the metastability of low-temperature $2s^2S_{1/2}$ compared to the high-temperature component. As mentioned above, the experimental result shown in Fig. 8 is understood qualitatively by the assumption that the metastability of the $2s^2S_{1/2}$ state is disturbed by collisions with electron and molecular hydrogen; however, this feature is not explained quantitatively based on the collision cross sections and the rate coefficients. Further investigations are necessary to obtain a better understanding of the mechanism underlying the less effective metastability of the $2s^2S_{1/2}$ state in plasma.

4.2. Origin of high-temperature $2s^2S_{1/2}$

The observation of high-temperature hydrogen atoms in plasma has been reported in several studies [11–18]. High-temperature hydrogen atoms can be detected by observing the Doppler-shifted component in the optical emission spectra of Balmer lines, which indicates the energy of excited ($n \geq 3$) hydrogen atoms. A kinetic energy higher than the electron temperature was observed, and several mechanisms were considered in the reported papers. For example, hydrogen ions are accelerated in a sheath electric field in front of a metal electrode with a negative potential. Ions are backscattered or reflected on the electrode surface, followed by dissociation or charge exchange collision resulting in atomic hydrogen. In addition, because super-hot hydrogen atoms are observed rather easily in hydrogen-argon mixture plasma, the energy transfer processes from argon ion and metastable argon are discussed. However, the mechanisms discussed in [11–18] are not adapted to the absorption spectra shown in Figs. 4 and 5, because the high-temperature component is observed only in the velocity distribution function of the $2s^2S_{1/2}$ state. In addition, the temperature of 2000-3000 K is significantly lower than that of atomic hydrogen reported in [11–18].

A likely mechanism for the high-temperature $2s^2S_{1/2}$ state observed in this study is the dissociative excitation of molecular hydrogen. Experimental evidence of the dissociative excitation is shown in Fig. 7, where we observed that the population of high-temperature $2s^2S_{1/2}$ was proportional to the electron density. This result was consistent with the assumption that $2s^2S_{1/2}$ was produced from molecular hydrogen in a one-step process. In contrast, the populations of $2p^2P_{1/2}$, $2p^2P_{3/2}$, and low-temperature $2s^2S_{1/2}$ were proportional to the square of the electron density, suggesting the production via a two-step process, where the first and second steps are $H_2 + e \rightarrow H + H + e$ and $H + e \rightarrow H^* + e$, respectively. Studies using time-of-flight measurements have reported two energy components in $2s^2S_{1/2}$ produced via dissociative excitation [19–21]. According to Misakian and Zorn [20], the first component has an energy of approximately 0.3 eV which is produced by electron impact with a threshold energy of 14.6 eV, and the other component has an energy of 4 eV, which has a threshold energy of 29 eV. It is reasonable to consider that the former is dominant in the low-temperature plasma used in the present study, and the energy of 0.3 eV is rather close to the temperature of the high-temperature $2s^2S_{1/2}$.

The reason why the high-temperature component is found only in the velocity distribution function of $2s^2S_{1/2}$ is understood by considering the lifetime of $2s^2S_{1/2}$ and the radiation trapping at the Lyman-α line. The $2p^2P_{1/2}$ and $2p^2P_{3/2}$ states with high

temperatures are probably produced simultaneously with $2s^2S_{1/2}$, but their lifetime is shorter than 2 ns because of the Lyman-α transition to the ground state. Since the Lyman-α line is optically thick, photons produced by the Lyman-α transition are absorbed by ground-state atomic hydrogen in the plasma, resulting in the excitation of the ground-state atomic hydrogen to $2p^2P_{1/2}$ and $2p^2P_{3/2}$. This indicates an interchange between the ground state and $2p^2P_{1/2,3/2}$ via radiation trapping. It is important to note here that the radiation trapping produces only the low-temperature (400 K) $2p^2P_{1/2}$ and $2p^2P_{3/2}$ states. Because ground-state atomic hydrogen is produced via the dissociation of molecular hydrogen, it may have a high energy at birth. However, because ground-state atomic hydrogen has a long lifetime, high-energy hydrogen atoms in the ground state relax (thermalize) via elastic collisions, resulting in a single temperature of 400 K. The $2p^2P_{1/2}$ and $2p^2P_{3/2}$ states produced by radiation trapping have the same temperature as the ground state. Because radiation trapping is a major production process for $2p^2P_{1/2}$ and $2p^2P_{3/2}$, the high-temperature component is not observed in their velocity distribution functions. In contrast, a lifetime longer than 100 ns is expected for $2s^2S_{1/2}$ according to the quenching frequency discussed in Section 4.1, and radiation trapping does not produce $2s^2S_{1/2}$. This may explain why the high-temperature component is observed only in the velocity distribution function of $2s^2S_{1/2}$.

5. Summary

In the present work, we examined the populations and the temperatures of the $2s^2S_{1/2}$, $2p^2P_{1/2}$, and $2p^2P_{3/2}$ states of atomic hydrogen in a low-density inductively coupled hydrogen plasma by analyzing the laser absorption spectrum of the Balmer-α line. The absorption spectrum agreed well with the theoretical spectrum when we assumed a population distribution deviated from the statistical weights and a high-temperature component in the velocity distribution function of $2s^2S_{1/2}$. It is reasonable to assume that the origin of high-temperature $2s^2S_{1/2}$ is the dissociative excitation of molecular hydrogen, and the negligible high-temperature components of $2p^2P_{1/2}$ and $2p^2P_{3/2}$ are attributable to the interchange with ground-state atomic hydrogen via radiation trapping. The metastability of $2s^2S_{1/2}$ was observed only in the high-temperature component at a low electron density ($n_e \leq 1 \times 10^{16}$ m^{-3}) and a low hydrogen pressure ($P \leq 20$ mTorr). The metastability was disturbed by increases in the electron density and hydrogen pressure, which can be understood qualitatively owing to collisional loss. However, from the quantitative point of view, the disturbance of the metastability was more significant than that expected by collision cross-sections. In addition, the experimental results suggest lower metastability of low-temperature $2s^2S_{1/2}$ than high-temperature one, which cannot be explained by collision cross-sections. A more sophisticated model should be investigated in future studies to obtain a better understanding of the kinetics of the $2s^2S_{1/2}$, $2p^2P_{1/2}$, and $2p^2P_{3/2}$ states.

References

[1] NIST Atomic Spectra Database, https://www.nist.gov/pml/atomic-spectra-database

[2] Shapiro J and Breit G 1959 *Phys. Rev.* **113** 179-181
[3] Biraben F, Garreau J C, Julien L and Ailegrini M 1990 *Rev. Sci. Instrum.* **61** 1468-1473
[4] Vetterhöffer J, Campargue A, Chenevier M and Stoeckel F 1993 *Diam. Relat. Mater.* **2** 481-485
[5] Lipp M R and O'Brien J J 1995 *Chem. Phys.* **192** 355-365
[6] Rousseau A, Teboul E and Sadeghi N 2004 *Plasma Sources Sci. Technol.* **13** 166-176
[7] Aramaki M, Okumura Y, Goto M, Muto S, Morita S and Sasaki K 2005 *Jpn. J. Appl. Phys.* **44** 6759-6763
[8] van Harskamp W E N, Brouwer C M, Schram D C, van de Sanden M C M and Engeln R 2012 *Plasma Sources Sci. Technol.* **21** 024009
[9] Merk F, Friedl R, Briefi S, Fröhler-Bachus C and Fantz U 2021 *Plasma Sources Sci. Technol.* **30** 065013
[10] Nishiyama S, Takada K and Sasaki K 2021 *Jpn. J. Appl. Phys.* **60** 076001
[11] Barbeau C and Jolly J 1990 *J. Phys. D: Appl. Phys.* **23** 1168-1174
[12] Kuraica M and Konjevic N 1992 *Phys. Rev. A* **46** 4429-4432
[13] Djurović S and Roberts J R 1993 *J. Appl. Phys.* **74** 6558-6565
[14] Adamov M R G, Obradović B M, Kuraica M M and Konjević N 2003 *IEEE Trans. Plasma Sci.* **31** 444-454
[15] Tatarova E, Felizardo E, Dias F M, da Silva M L, Ferreira C M and Gordiets B 2009 *Appl. Phys. Lett.* **95** 181503
[16] Akhtar K, Scharer J E and Mills R L 2009 *J. Phys. D: Appl. Phys.* **42** 135207
[17] Mills R L and Akhtar K 2010 *Int. J. Hydrogen Energ.* **35** 2546-2555
[18] Marchuk O, Brandt C, Pospieszczyk A, Reinhart M, Brezinsek S, Unterberg B and Dickheuer S 2018 *J. Phys. B: At. Mol. Opt. Phys.* **51** 025702
[19] Leventhal M, Rosiscoe R T and Lea K R 1967 *Phys. Rev* **158** 49-56
[20] Misakian M and Zorn J C 1972 *Phys. Rev. A* **6** 2180-2196
[21] Ryan S R, Spezeski J J, Kalman O F, Lamb Jr. W E, McIntyre, Jr. L C and Wing W H 1979 *Phys. Rev. A* **19** 2192-2196
[22] Ajello J M, Ahmed S M, Kanik I and Multari R 1995 *Phys. Rev. Lett* **75** 3261-3264
[23] Ajello J M, Ahmed S M and Liu X 1996 *Phys Rev. A* **53** 2303-2308
[24] Ito K, Oda N, Hatano Y and Tsuboi T 1976 *Chem. Phys.* **17** 35-43
[25] Higo M, Kamata S and Ogawa T 1982 *Chem. Phys.* **66** 243-248
[26] Demtröder W 2008 *Laser Spectroscopy Vol. 1, Fourth edition* (Springer) p.22.
[27] Demtröder W 2008 *Laser Spectroscopy Vol. 2, Fourth edition* (Springer) p.98.
[28] Janev R K, Langer W D, Evans, Jr. K and Post, Jr. D E 1987 *Elementary Processes in Hydrogen-Helium Plasmas* (Springer) p.23.
[29] Ryan, S R, Czuchlewski S J and McCusker M V 1977 *Phys. Rev. A* **16** 1892-1905
[30] Weissmann W, Hartmann W and Burch D S 1987 *Z. Phys. D-Atoms, Molecules and Clusters* **7** 119-123
[31] Glass-Maujean M 1989 *Phys. Rev. Lett.* **62** 144-146
[32] Vassilev G, Perales F, Miniatura Ch, Robert J, Reinhardt J, Vecchioeattivi F and Baudon J 1990 *Z. Phys. D-Atoms, Molecules and Clusters* **17** 101-107
[33] Rowland R S and Taylor R 1996 *J. Phys. Chem.* **100** 7384-7391

Table 1. Wavelengths and transition probabilities of the seven fine structure components of the Balmer-α line of atomic hydrogen, together with the lower and upper energy states.

Label	Wavelength (nm)	Transition probability (s^{-1})	Lower state	Upper state
A	656.291	4.21×10^6	$2p\,^2P^o_{3/2}$	$3s\,^2S_{1/2}$
B	656.287	1.08×10^7	$2p\,^2P^o_{3/2}$	$3d\,^2D_{3/2}$
C	656.285	6.47×10^6	$2p\,^2P^o_{3/2}$	$3d\,^2D_{5/2}$
D	656.277	2.24×10^7	$2s\,^2S_{1/2}$	$3p\,^2P^o_{1/2}$
E	656.275	2.10×10^6	$2p\,^2P^o_{1/2}$	$3s\,^2S_{1/2}$
F	656.272	2.24×10^7	$2s\,^2S_{1/2}$	$3p\,^2P^o_{3/2}$
G	656.271	5.39×10^7	$2p\,^2P^o_{1/2}$	$3d\,^2D_{3/2}$

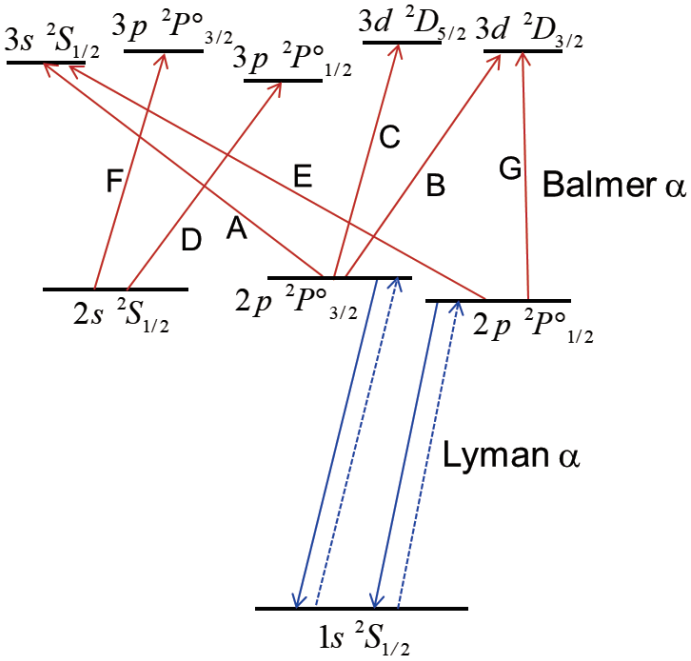

Figure 1. Partial energy level diagram of atomic hydrogen related to the Lyman-α and Balmer-α transitions.

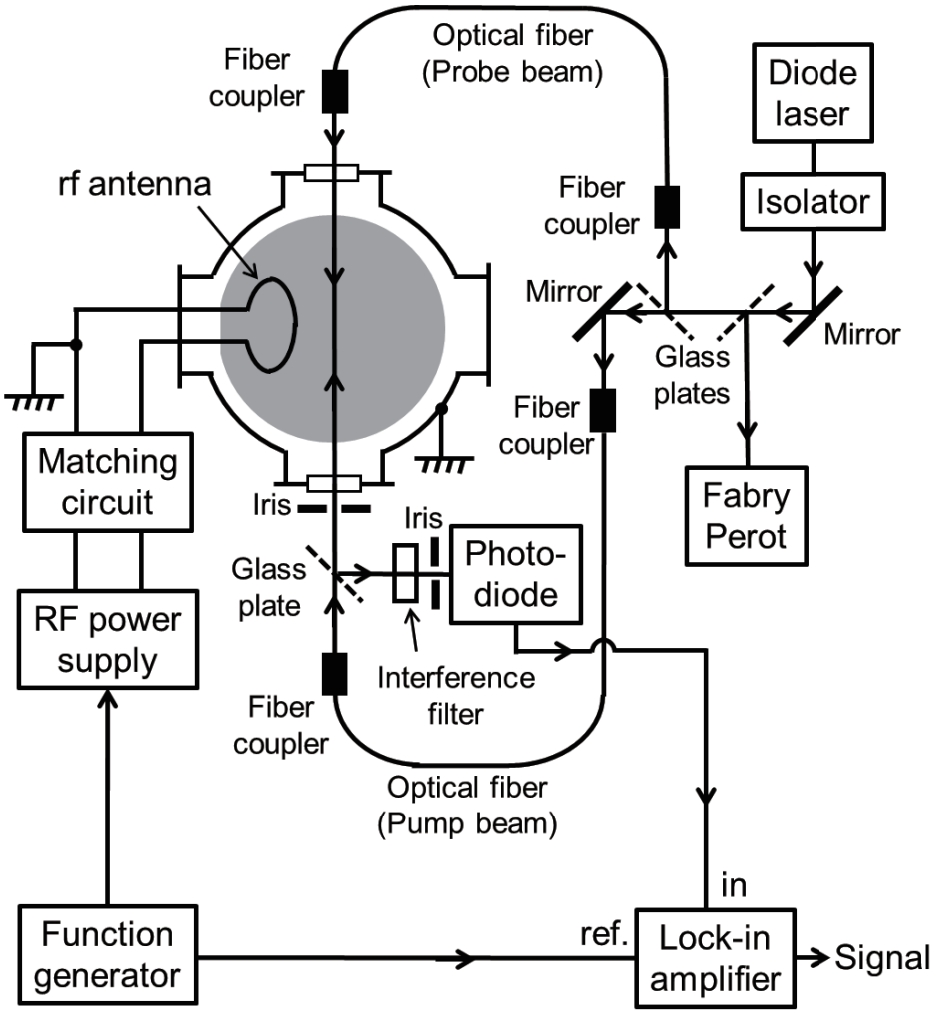

Figure 2. Schematic illustration of experimental setup. Inductively coupled hydrogen plasma was generated by applying RF power to an antenna inserted in a vacuum chamber. The output from a diode laser was divided into pump and probe beams. Both the pump and probe beams were used for measuring the Lamb-dip spectrum by saturated absorption spectroscopy, while the pump beam was blocked when measuring the Doppler-broadened absorption spectrum.

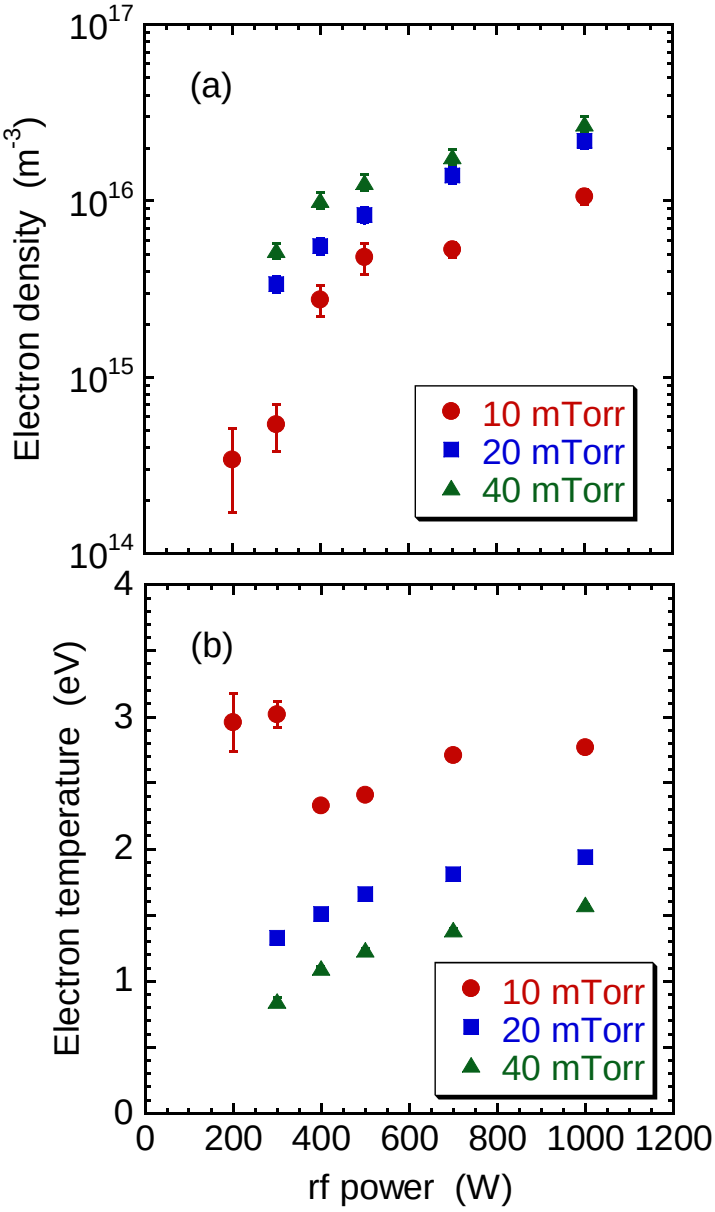

Figure 3. (a) Electron density and (b) electron temperature as a function of the RF power. The measurements were repeated at hydrogen pressures of 10, 20, and 40 mTorr.

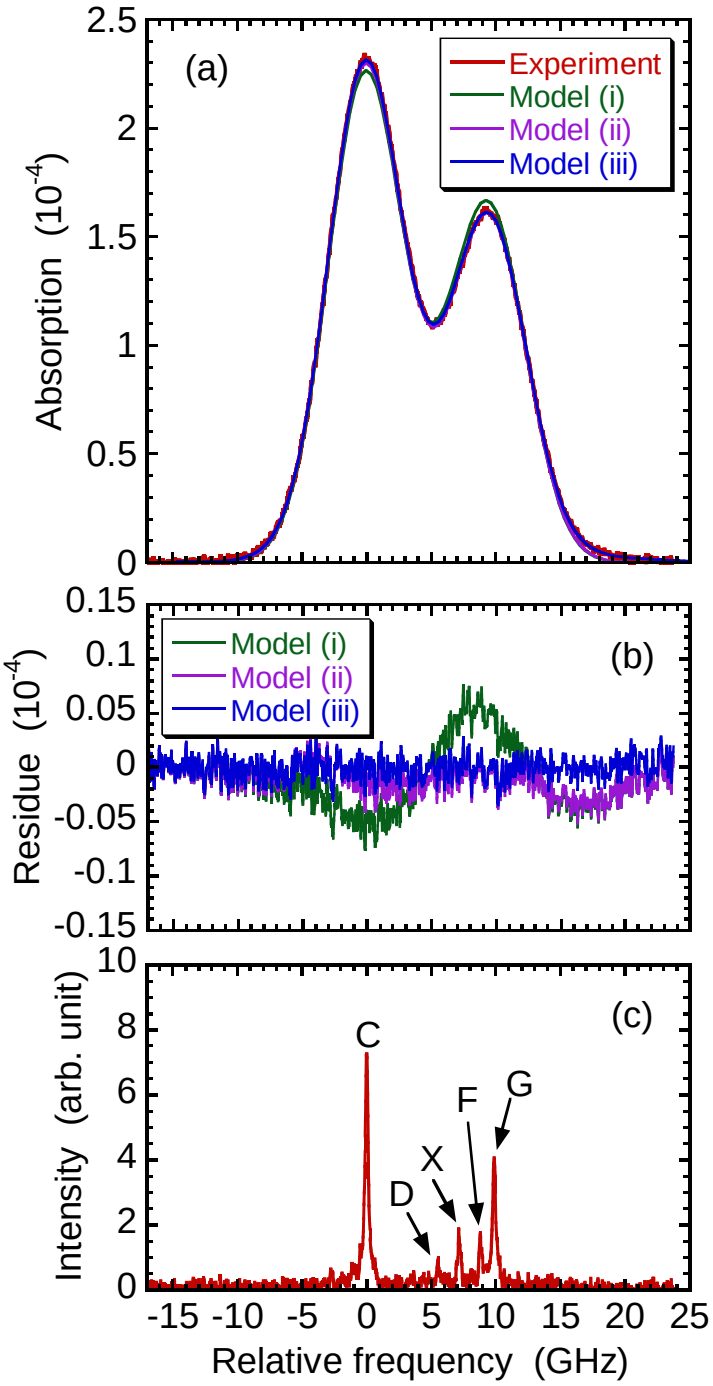

Figure 4. (a) Doppler broadened absorption spectrum of the Balmer-α line observed at an RF power of 700 W and a hydrogen pressure of 40 mTorr, together with the fittings with theoretical spectra using models (i)-(iii). (b) Residue between the experimental and fitting spectra. (c) Lamb-dip spectrum obtained by saturated absorption spectroscopy. The alphabetical characters correspond to the transitions shown in Fig. 3, and peak X is the cross over between peaks D and F.

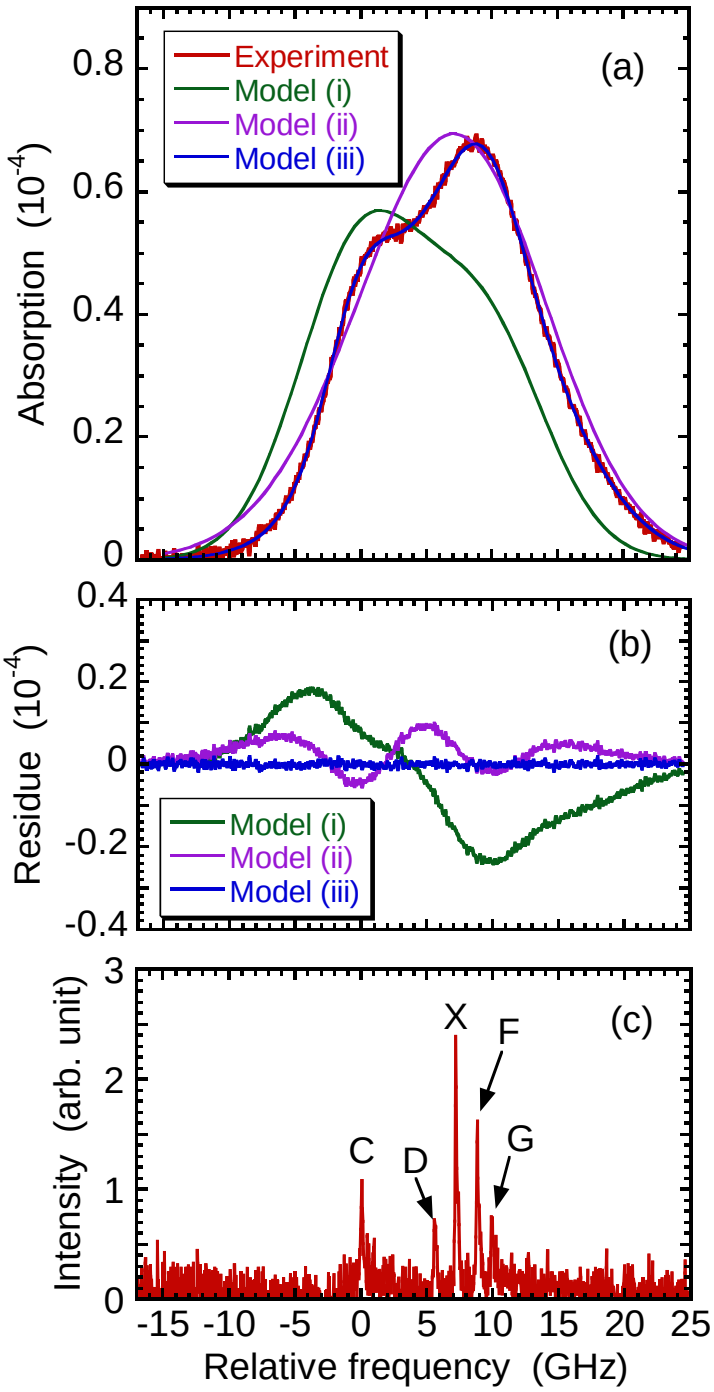

Figure 5. Same as Fig. 4, except that the hydrogen pressure was 20 mTorr.

.

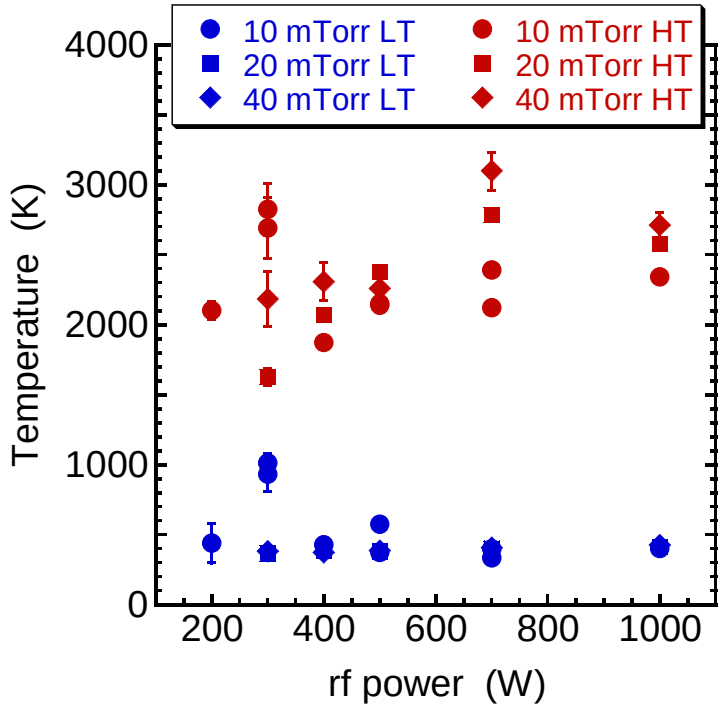

Figure 6. Temperatures of the high-temperature component of $2s^2S_{1/2}$ (HT) and the low-temperature components of $2s^2S_{1/2}$, $2p^2P_{1/2}$, and $2p^2P_{3/2}$ (LT) as a function of the RF power. The measurements were repeated at hydrogen pressures of 10, 20, and 40 mTorr.

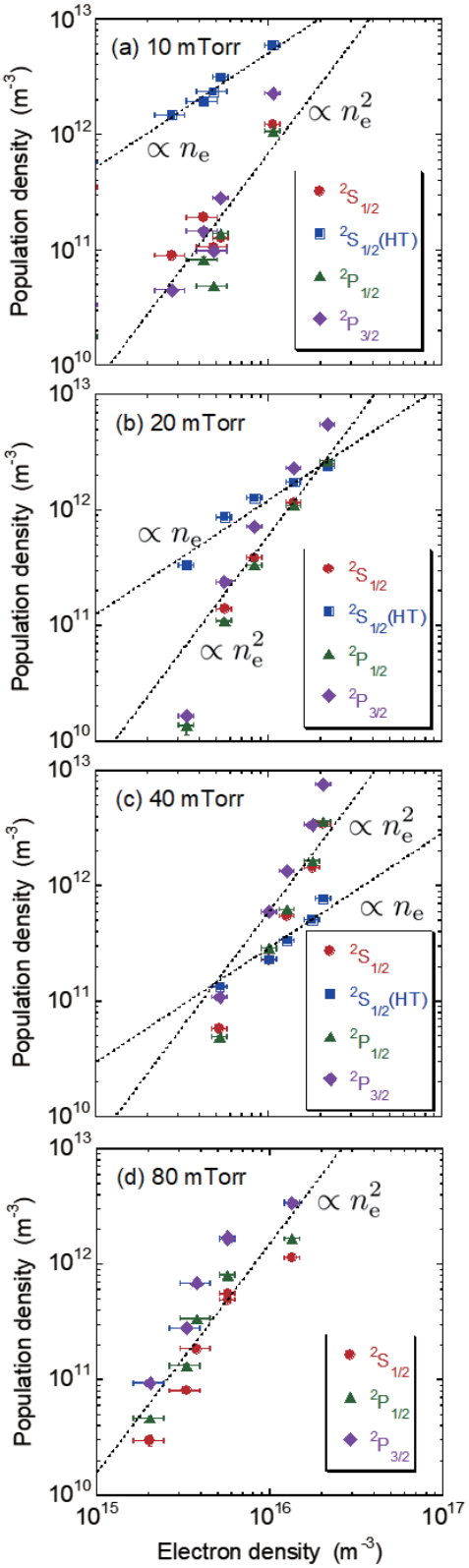

Figure 7. Populations of the high-temperature component of $2s^2S_{1/2}$ and the low-temperature components of $2s^2S_{1/2}$, $2p^2P_{1/2}$, and $2p^2P_{3/2}$ as a function of the electron density. The hydrogen pressures were (a) 10 mTorr, (b) 20 mTorr, (c) 40 mTorr, and (d) 80 mTorr. The high-temperature component of $2s^2S_{1/2}$ is not plotted in (d) since its population was negligible at 80 mTorr.

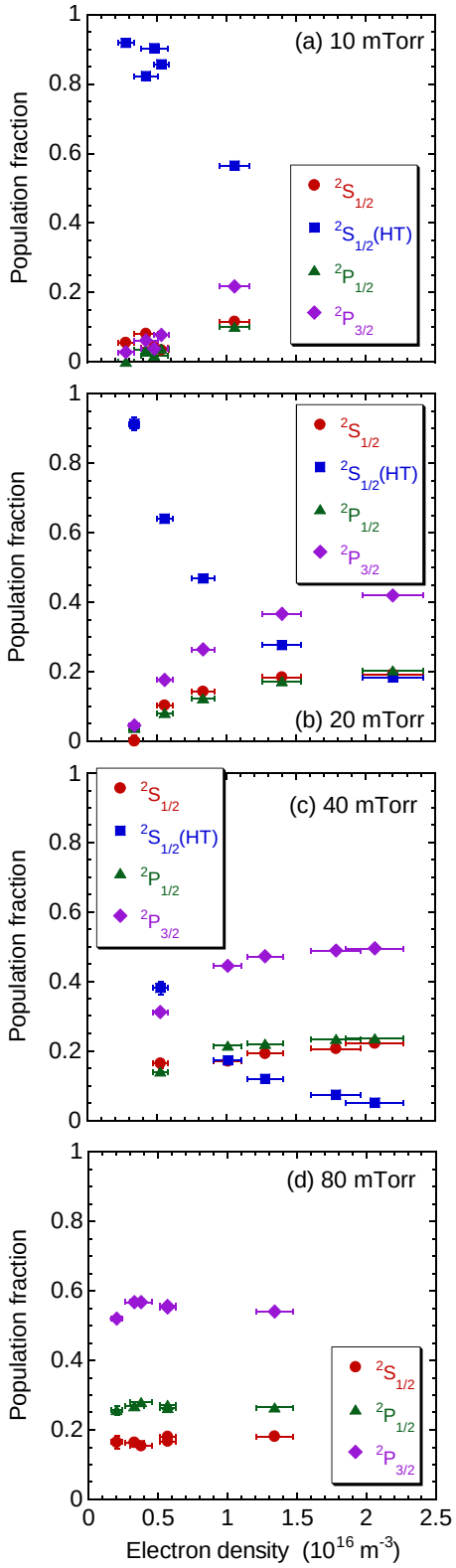

Figure 8. Fractional abundances of the high-temperature component of $2s^2S_{1/2}$ and the low-temperature components of $2s^2S_{1/2}$, $2p^2P_{1/2}$, and $2p^2P_{3/2}$ as a function of the electron density. The hydrogen pressures were (a) 10 mTorr, (b) 20 mTorr, (c) 40 mTorr, and (d) 80 mTorr. The high-temperature component of $2s^2S_{1/2}$ is not plotted in (d) since its population was negligible at 80 mTorr.